Journal of Materials Science: Materials in Electronics (2020) 31:2544–2550
https://doi.org/10.1007/s10854-019-02791-y

A new additive-free microwave dielectric ceramic system for LTCC applications: $(1-x)CaWO_4-x(Li_{0.5}Sm_{0.5})WO_4$

Xueqi Hu[1] · Juan Jiang[1] · Jinzhao Wang[1] · Lin Gan[1] · Tianjin Zhang[1]

Received: 17 October 2019 / Accepted: 19 December 2019 / Published online: 2 January 2020

Abstract
In this work, a novel additive-free microwave dielectric ceramic (MWDC) system of $(1-x)CaWO_4-x(Li_{0.5}Sm_{0.5})WO_4$ (CW-LSW, $0.12 \le x \le 0.20$) for low temperature co-fired ceramic (LTCC) applications was successfully fabricated by a solid-state reaction route. The sintering temperature and composition effects on the microwave dielectric (MWD) properties, microstructures, and crystalline phases were investigated. The optimal sintering temperatures of the CW-LSW ceramics are ranging from 875 to 950 °C. When sintered at 900 °C for 3 h, the sample of 0.86CW-0.14LSW exhibited excellent MWD properties: $\varepsilon_r = 10.76$, $Q \times f = 28{,}754$ GHz, and $\tau_f = -0.54$ ppm/°C. Furthermore, it is found that the CW-LSW ceramics are well compatible with Ag electrode during the sintering process. Therefore, the findings suggest that CW-LSW ceramic materials are promising for LTCC applications.

1 Introduction

Low temperature co-fired ceramic (LTCC) materials have aroused increasing international interest because of their promising applications in electronic industry [1]. As known to all, the LTCC materials are widely applied to many microwave devices, including antennas, filters, oscillators, dielectric waveguides, and substrates [2–4]. To meet the requirements of the applications mentioned above, it is necessary for the LTCC materials to have a combination of a near-zero temperature coefficient of resonant frequency (τ_f), a high quality factor ($Q \times f$), and a low dielectric constant (ε_r) [5, 6]. Moreover, in order to be co-fired with electrode metals (e.g., Au, Ag, and Cu), the sintering temperatures of the LTCC materials have to be lower than the melting points of metal electrodes (e.g., < 950 °C) [7, 8]. Therefore, effective sintering additives, such as H_3BO_3, Li_2CO_3, $BaCu(B_2O_5)$, and low-melting glass were usually employed to decrease the sintering temperature. However, as a result of the formation of secondary phases, glassy phases, and structural defects caused by the use of the sintering additives, the $Q \times f$ value will be inevitably decreased, which significantly hinders the applications of the LTCC materials [2–4, 9, 10]. Consequently, it is highly necessary to study the fabrication of additive-free LTCC materials with high $Q \times f$ values.

However, it is quite challenging to develop additive-free LTCC materials, as relatively few ceramic materials can be fully sintered at temperatures lower than 950 °C without any additive [5, 11–18]. Recently, tungstate ceramic materials (e.g., $CaWO_4$, $SrWO_4$, and $BaWO_4$) were found to be excellent candidates for LTCC applications and therefore be intensively studied [19]. Among these tungstate ceramic materials, $CaWO_4$ with a scheelite structure presented outstanding microwave dielectric (MWD) properties (i.e., $\varepsilon_r = 10$, $Q \times f = 75{,}000$ GHz, and $\tau_f = -25$ ppm/°C) [19, 20]. Although the sintering temperature of $CaWO_4$ is at about 1100 °C, it is easy to be effectively decreased by combining $CaWO_4$ with some other tungstate materials, which have lower sintering temperatures. As reported by Zhang et al., a high $Q \times f$ value (i.e., 117,600 GHz), a low dielectric constant (i.e., 9), and a relatively large negative τ_f (i.e., − 55 ppm/°C) were achieved in the binary ceramic system of $CaWO_4$-Li_2WO_4, when sintered at 900 °C [12]. Furthermore, as shown by Bian et al. with an addition of $(Li_{0.5}Nd_{0.5})WO_4$, low sintering temperatures

✉ Lin Gan
ganlin@hubu.edu.cn

✉ Tianjin Zhang
zhangtj@hubu.edu.cn

[1] Hubei Collaborative Innovation Center for Advanced Organic Chemical Materials, Ministry of Education Key Laboratory for the Green Preparation and Application of Functional Materials and School of Material Science and Engineering, Hubei University, 368 Youyi Avenue, Wuhan 430062, China

and a near-zero τ_f level were achieved simultaneously in the $CaWO_4$-based ceramics (when sintered at 825 °C, $\varepsilon_r = 11.7$, $Q \times f = 36{,}700$ GHz, and $\tau_f = 5.36$ ppm/°C) [21]. Similarly, $(Li_{0.5}Sm_{0.5})WO_4$ ($\varepsilon_r = 17$, $Q \times f = 5792$ GHz, $\tau_f = 86.7$ ppm/°C, sintered at 800 °C) is also expected to be an excellent additive simultaneously to tailor the τ_f level and lower the sintering temperature of $CaWO_4$ ceramic materials [22].

In the present study, specimens of a novel additive-free LTCC system of $(1-x)CaWO_4$–$x(Li_{0.5}Sm_{0.5})WO_4$ (CW-LSW) were prepared. The influences of the composition and sintering temperature on the MWD properties, microstructures and crystalline phases of the ceramic specimens were studied. Additionally, the compatibility of the ceramic samples with Ag was also investigated.

2 Experimental procedure

Ceramic specimens of $(1-x)$CW-xLSW ($x = 0.12$, 0.14, 0.16, 0.18, and 0.20) were prepared via a conventional solid-state reaction route. The raw materials were highly pure powders of Sm_2O_3 (99.9%, Zibo Weijie, China), Li_2CO_3 (99.9%, Shanghai Oujin, China), $CaCO_3$ (99.9%, Sinopharm, China), and WO_3 (99.9%, Shanghai Zaibang, China). Initially, according to the compositions of $CaWO_4$ and $(Li_{0.5}Sm_{0.5})WO_4$, the starting powders were weighed and were milled in anhydrous alcohol for 8 h. After that, drying of the slurries was carried out at 90 °C. The precursors of $CaWO_4$ and $(Li_{0.5}Sm_{0.5})WO_4$ were heated for 3 h at 850 and 670 °C, respectively. The as-prepared powders were weighed according to the composition of $(1-x)$CW-xLSW, and were ball-milled and dried again. Then 10 wt% polyvinyl alcohol solution (PVA, 5 wt%) was added into the mixtures. The powders were pressed into Φ17 mm green bodies (~ 11 mm in thickness) in a steel mold. Debinding was performed at 550 °C for 3 h in air. Sintering was conducted at various temperatures (i.e., 775 to 975 °C) for 4 h in air. The chemical compatibility with Ag was evaluated by co-firing the green bodies with Ag powder in air at 900 °C for 4 h.

X-ray powder diffraction analyses (XRD, D8 advance, Bruker, Germany) were employed for phase identification. The lattice parameters of the specimens were calculated according to the XRD results. A scanning electron microscope (SEM, JSM-7100F, JEOL, Japan) was used for microstructural observations, corresponding composition analyses were performed using an energy dispersive spectrometer (EDS, IE250, Oxford Instruments, UK). The Archimedes method was employed to determine the bulk densities of the specimens. Calculation of the theoretical densities of the specimens was carried out according to the measured lattice parameters. The relative densities were obtained according to the results of the bulk density and theoretical density. The theoretical density was calculated using Eq. 1,

$$\rho_{\text{the}} = \frac{M_x \cdot Z}{V \cdot N_A}, \tag{1}$$

where Mx is the molecular weight, V is the cell volume calculated according to the XRD results, N_A is the Avogadro constant, and $Z = 4$. The relative density was calculated using Eq. 2,

$$\rho_{\text{rel}} = \frac{\rho_{\text{ap}}}{\rho_{\text{the}}} \times 100\%, \tag{2}$$

where ρ_{ap} and ρ_{the} are the bulk density and the relative density, respectively. The MWD properties of the ceramics were analysed using a network analyser (E5071C, Agilent, US) with the $TE_{01\delta}$ shielded cavity reflection method. The τ_f value was calculated using Eq. 3,

$$\tau_f = \frac{f_{(T_2)} - f_{(T_1)}}{f_{(T_1)}(T_2 - T_1)} \times 10^6 (\text{ppm/°C}), \tag{3}$$

where $f_{(T_1)}$ and $f_{(T_2)}$ are the resonant frequencies measured at − 20 and 65 °C, respectively. The packing fraction of a scheelite unit cell ($A^{2+}B^{6+}O_4$) was obtained using Eq. 4,

$$\begin{aligned} \text{packing fraction}(\%) &= \frac{\text{volume of packed ions}}{\text{volume of primitive unit cell}} = \frac{\text{volume of packed ions}}{\text{volume of unit cell}} \times Z \\ &= \frac{4\pi/3 \times \left(r_A^3 + r_B^3 + r_O^3 \times 4\right)}{a^2 \times c} \times 4, \end{aligned} \tag{4}$$

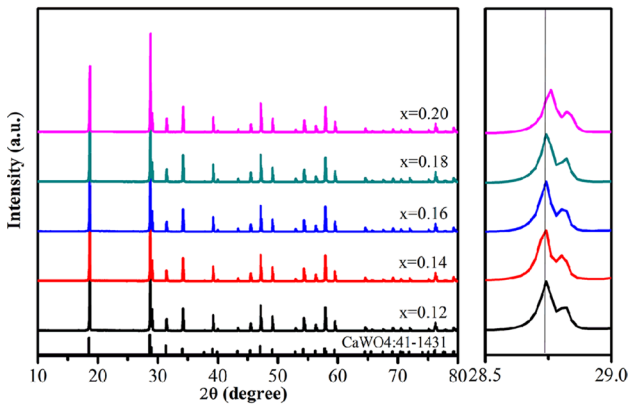

Fig. 1 XRD results of the $(1-x)$CW-xLSW specimens with different x values sintered at 900 °C

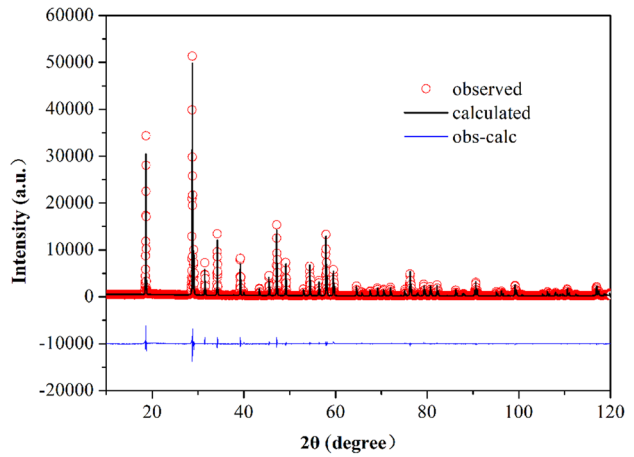

Fig. 2 Calculated (line) and experimental (circles) XRD patterns of the 0.86CW-0.14LSW sample (the bottom line is the difference between the calculated and the observed intensity)

Table 1 Lattice parameters of the $(1-x)$CW-xLSW ceramic samples with various x values

x value	a (Å)	c (Å)	V (Å^3)
0.12	5.24345	11.36675	312.51427
0.14	5.24302	11.36375	312.38078
0.16	5.24307	11.36243	312.35089
0.18	5.24292	11.36084	312.28887
0.20	5.24289	11.35943	312.24639

where a and c are the calculated lattice parameters, r_A, r_B and r_O are the ionic radii, and $Z=4$ [23].

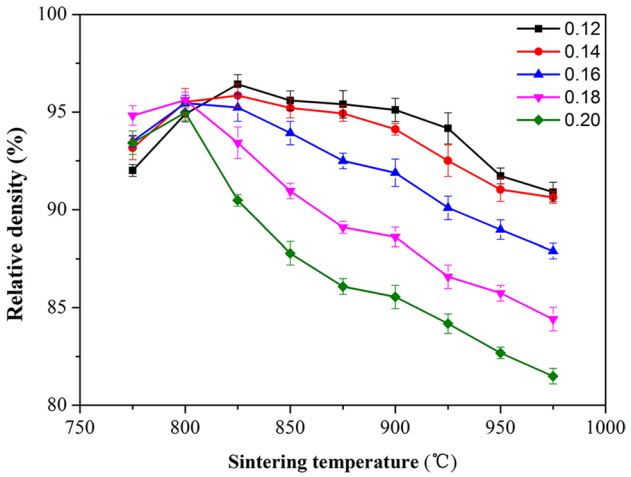

Fig. 3 Relative density of the $(1-x)$CW-xLSW $(0.12 \le x \le 0.20)$ specimens sintered at different temperatures

3 Results and discussion

XRD results of the $(1-x)$CW-xLSW $(0.12 \le x \le 0.20)$ ceramic specimens fabricated at 900 °C are shown in Fig. 1. Obviously, all the specimens exhibited a single tetragonal scheelite phase, indicating the formation of solid solutions in the samples. This should be mainly attributed to that both $CaWO_4$ and $(Li_{0.5}Sm_{0.5})WO_4$ have the same scheelite structure. Additionally, the diffraction peaks of the samples gradually shifted to higher angles as the x value increased, which suggests a continuous lattice shrinkage caused by the partial replacement of the large Ca^{2+} ions ($r=1.12$ Å, CN = 8) by the smaller $(Li_{0.5}Sm_{0.5})^{2+}$ ions (the average ion radius is 1.00 Å, CN = 8) [24].

The lattice parameters of the $(1-x)$CW-xLSW samples with various x values were calculated according to the XRD results. Figure 2 gives the representative refinement pattern ($x=0.14$), the obtained refinement parameters are $R_p=8.75$, $R_{wp}=10.84$, and $R_{exp}=4.22$. The refined lattice parameters and corresponding cell volumes are presented in Table 1. It can be seen that with an increment of x, both the lattice parameters of a and c decreased monotonously, which gave rise to the shrinkage of the cell volume of the samples. This phenomenon is in consistence with the XRD peak shift towards higher angles (see Fig. 1).

Figure 3 illustrates the relative densities of the $(1-x)$CW-xLSW $(0.12 \le x \le 0.20)$ specimens sintered at various temperatures. Clearly, relatively high densities (i.e., > 90%) were already obtained in all compositions when sintered at 775 °C. As the sintering temperature rised from 775 to 975 °C, the relative densities of all these samples initially increased and then decreased. A possible reason for the unusual decrease can be ascribed to partial evaporation of some of the raw materials (e.g., Li_2O) at elevated temperatures

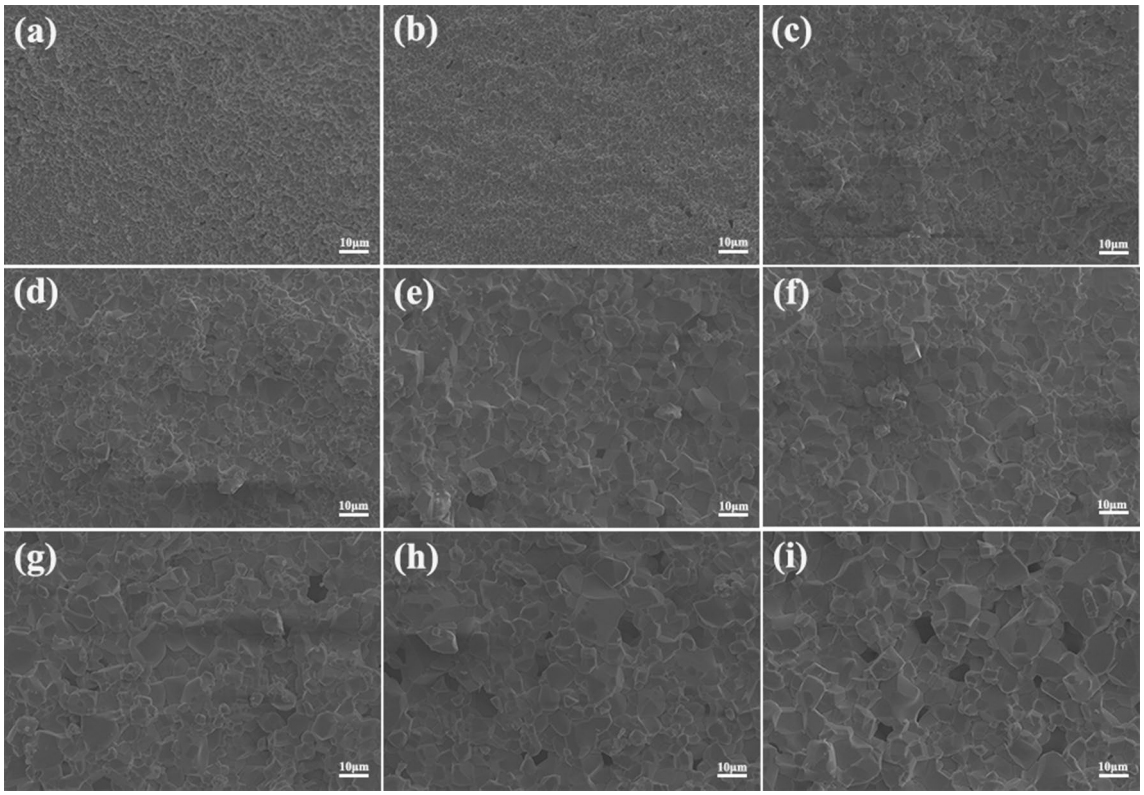

Fig. 4 SEM graphs of the samples with $x = 0.14$ fabricated at different temperatures of **a** 775, **b** 825, **c** 875, **d** 900 and **e** 950 °C; and the specimens sintered at 950 °C with different x values of **f** 0.12, **g** 0.16, **h** 0.18, and **i** 0.20

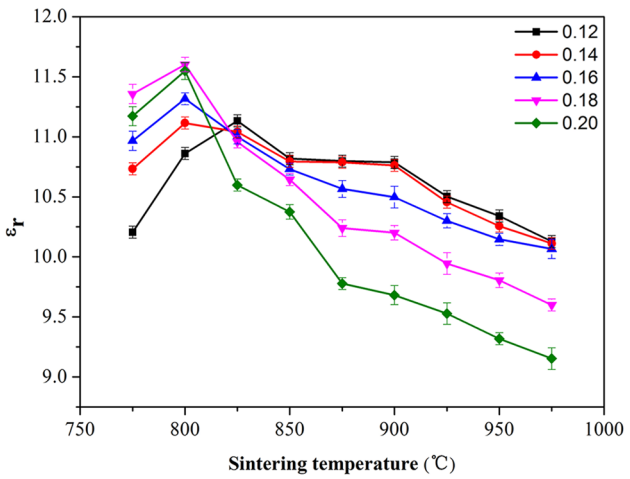

Fig. 5 ε_r of the $(1-x)$CW-xLSW $(0.12 \le x \le 0.20)$ ceramic samples sintered at different temperatures

[25, 26]. Furthermore, x also had a remarkable effect on the relative densities of the samples, when the sintering temperature was fixed, the density level decreased as x increased.

To investigate the microstructural evolution of the CW-LSW ceramic samples, SEM observations were performed. SEM photographs of the ceramics with $x = 0.14$ prepared at different temperatures are presented in Fig. 4a–e. It was found that when sintered at only 775 °C, the sample was already well densified, only a small amount of residual pores were observed with a fine average grain size (~2.5 μm, see Fig. 4a). With further increases in the sintering temperature to 875, 900 and 950 °C, the residual pores were not effectively eliminated, meanwhile, as the sintering temperature increased, both the pore size and grain size increased remarkably (see Fig. 4a–e). Moreover, the above samples were homogeneous in their grain sizes, no apparent abnormal grain growth was observed. The compositional effects on the microstructures of the samples were also investigated. Figure 4e–i gives the SEM images of the specimens sintered at 950 °C with various x levels. Obviously, as x increased, the grain size of the specimens exhibited no apparent change, while a remarkable increase in the amount of the residual pores was clearly observed. These SEM observation results are in consistence with the variation of the relative densities of the specimens.

Figure 5 gives the variation of the ε_r levels of the $(1-x)$CW-xLSW $(0.12 \le x \le 0.20)$ specimens as a function of the sintering temperature. As the sintering temperature rised from 775 to 975 °C, the variation of the ε_r levels of all compositions is in well agreement with that of the specimen densities (see Fig. 3). The maximal ε_r values of each

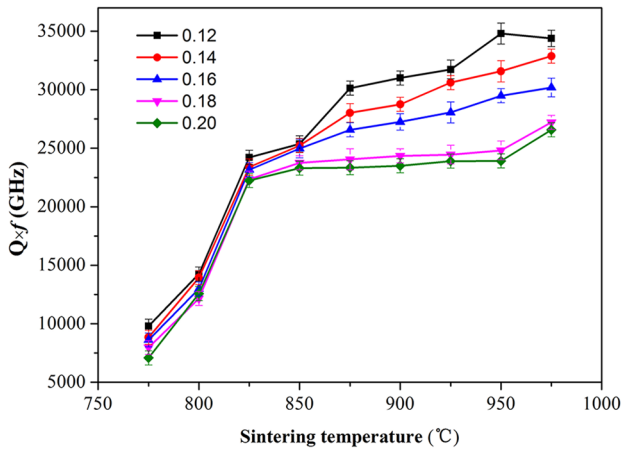

Fig. 6 Q×*f* levels of the (1 − *x*)CW-*x*LSW (0.12 ≤ *x* ≤ 0.20) samples sintered at various temperatures

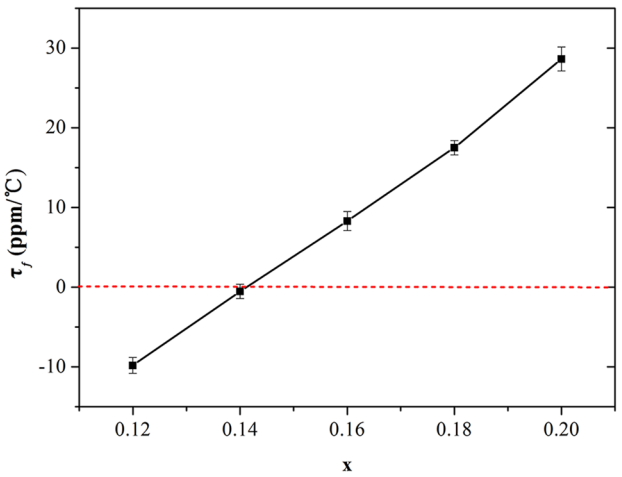

Fig. 7 τ_f levels of the (1 − *x*)CW-*x*LSW specimens with various x sintered at 900 °C

composition were achieved at 800 or 825 °C, at those temperatures the highest relative density levels were obtained, which is as a result of that the permittivity is strongly dependent on the relative density. In addition, the dielectric constants decreased as the *x* value increased. This decrease in the ε_r value has two causes; on one hand, the relative densities decreased with an increase in the *x* value (see Fig. 3). On the other hand, as the *x* value increased, more Ca^{2+} ions with higher ionic polarizability (i.e., 3.16 Å^3) were replaced by $(Li_{0.5}Sm_{0.5})^{2+}$ ions, which are lower in ionic polarizability (i.e., 2.97 Å^3) [5].

The Q×*f* levels of the (1 − *x*)CW-*x*LSW ceramic samples sintered at 775 to 975 °C are presented in Fig. 6. Obviously, the Q×*f* levels are strongly influenced by both the sintering temperature and composition. Generally, the Q×*f* of all specimens different in composition gradually increased as the sintering temperature increased. Moreover, when sintered at a fixed temperature, the Q×*f* levels decreased as the *x* value increased. The Q×*f* levels of MWD ceramic materials are closely related to some factors, such as secondary phases, impurities, porosity, grain size, and lattice defects [27]. The composition-dependent variation of the Q×*f* is partially ascribed to that the relative densities of the specimens decreased remarkably as *x* increased (see Fig. 3). Furthermore, as shown in Table 2, the packing fraction levels of the samples decreased with an increment of the *x* value, which also led to the deterioration of the Q×*f*. It is owing to that with a decrease in the packing fraction, the intensity of the lattice vibration increased. As a result, the intrinsic loss increased and the Q×*f* level decreased [23, 28]. It should be noted that although the relative densities of the specimens slightly decreased as the sintering temperature increased, this relatively limited variation had no apparent negative effect on the Q×*f* of the specimens. With an increase in sintering temperature, the relative density of ceramic samples decreased, and the porosity increased, which usually lead to a decrease in the Q×*f*. However, the quality factor increased. Therefore, some other factors competed with a decrease in the density and dominated the change of the Q×*f* value. As observed by SEM (see Fig. 4), the grain size of the samples had a significant increase with an increase in the sintering temperature, which may remarkably decrease the grain boundaries and suppress the dielectric loss [29, 30]. The specific reason of this phenomenon still needs further study.

Figure 7 exhibits the τ_f levels of the ceramics with different *x* levels sintered at 900 °C. Clearly, the τ_f levels increased monotonously from − 9.8 to 28.6 ppm/°C as

Table 2 Packing fractions of the (1 − *x*)CW-*x*LSW ceramic samples with various *x* values (r_O, r_A, and r_B, represent the effective ionic radii of the oxygen ions, A-site, and B-site cations at each coordination number, respectively)

x value	r_A (Å) (CN = 8)	r_B (Å) (CN = 4)	r_O (Å) (CN = 3)	Z	Packing fraction (%)
0.12	1.1056	0.42	1.36	4	61.59
0.14	1.1032	0.42	1.36	4	61.57
0.16	1.1008	0.42	1.36	4	61.53
0.18	1.0984	0.42	1.36	4	61.49
0.20	1.0960	0.42	1.36	4	61.45

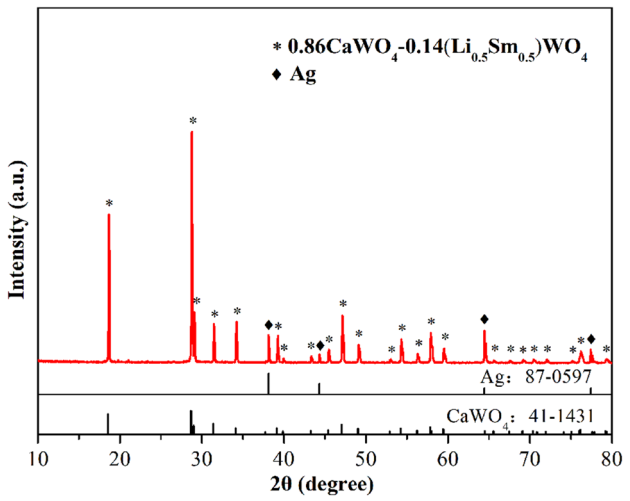

Fig. 8 XRD pattern of the 0.86CW-0.14LSW ceramic co-fired with Ag at 900 °C

x increased from 0.12 to 0.20. Moreover, a near-zero τ_f level (i.e., − 0.54 ppm/°C) was obtained when $x = 0.14$. As is well-known, $CaWO_4$ has a negative τ_f value (i.e., − 25 ppm/°C) [10], in contrast, $(Li_{0.5}Sm_{0.5})WO_4$ has a positive one (i.e., 86.7 ppm/°C) [22]. As a result, in the CW-LSW system, an increase in the $(Li_{0.5}Sm_{0.5})WO_4$ content (i.e., the x value) will result in an increment of the τ_f value from negative to positive [21, 31].

The chemical compatibility with Ag was evaluated via co-firing a ceramic sample ($x = 0.14$) with pure silver powder in ambient atmosphere at 900 °C. In the XRD pattern of the co-fired sample (see Fig. 8), the diffraction peaks of both silver and the scheelite phase were identified, and no impurity phase, such as Ag_2WO_4 or $Ag_2W_2O_7$ were detected. Additionally, as confirmed by the SEM observations combined with EDS analyses (see Fig. 9), the silver particles exhibited a homogeneous distribution on the surface of the ceramic sample. These results indicate that there was no apparent chemical reaction between Ag and the ceramic sample during the sintering process. Therefore, the $(1-x)$CW-xLSW ceramic materials were proved to be compatible with Ag electrodes.

As mentioned above, it is crucial for the LTCC materials to have a combination of low sintering temperatures, outstanding MWD properties, as well as excellent compatibility with metal electrodes. Undoubtedly, this study provides a promising candidate material system for LTCC technology. Meanwhile, it is worth to note that for the CW-LSW ceramic system, relatively high $Q \times f$ levels (~ 30,000 GHz) can be obtained in a wide range of the sintering temperature (i.e., 875–950 °C), which is quite favorable for practical applications. Additionally, in consideration of the relative density levels of the specimens (i.e., ~ 95%), further study can focus on increasing the relative density by optimizing the powder processing and sintering parameters, which is expected to effectively improve the $Q \times f$ of the CW-LSW ceramics.

4 Conclusions

In summary, samples of a new additive-free ceramic system of $(1-x)$CW-xLSW ($0.12 \le x \le 0.20$) were prepared. A single scheelite phase was detected in each specimen. The MWD properties of the $(1-x)$CW-xLSW specimens were strongly dependent on both the sintering temperature and composition. An increment of x (i.e., the content of $(Li_{0.5}Sm_{0.5})WO_4$) resulted in decreases in both the $Q \times f$ value and permittivity, as well as an increase in the τ_f level. A near-zero τ_f level of − 0.54 ppm/°C was achieved at $x = 0.14$ with $\varepsilon_r = 10.76$ and $Q \times f = 28{,}754$ GHz, when sintered at 900 °C. Moreover, the ceramic samples showed

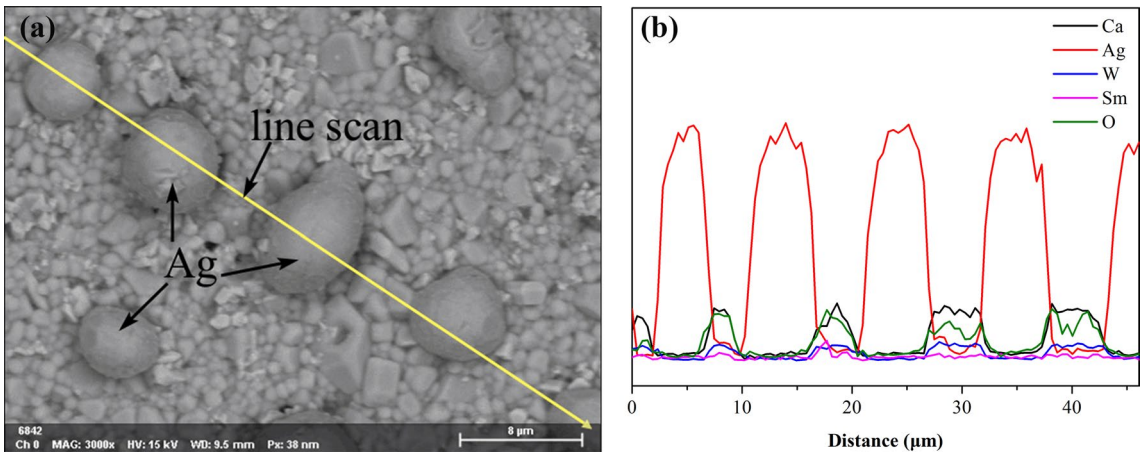

Fig. 9 **a** Back scattered electron image of the 0.86CW-0.14LSW ceramic co-fired with Ag at 900 °C; **b** EDS line-scan patterns from the observed surface of the co-fired sample

excellent chemical compatibility with Ag during the sintering process. The findings suggest that the CW-LSW ceramics are promising candidate materials for LTCC applications.

Acknowledgements This work was supported by the National Science Foundation of China (Nos. 11774083 and 51902093).

References

1. M.T. Sebastian, H. Jantunen, Low loss dielectric materials for LTCC applications: a review. Int. Mater. Rev. **53**(2), 57–90 (2013)
2. M. Guo, G. Dou, S. Gong, D. Zhou, Low-temperature sintered $MgWO_4$–$CaTiO_3$ ceramics with near-zero temperature coefficient of resonant frequency. J. Eur. Ceram. Soc. **32**(4), 883–890 (2012)
3. S. Zhang, H. Su, H. Zhang, Y. Jing, X. Tang, Microwave dielectric properties of $CaWO_4$–Li_2TiO_3 ceramics added with LBSCA glass for LTCC applications. Ceram. Int. **42**(14), 15242–15246 (2016)
4. Z. Zhang, H. Sun, X. Tang, H. Zhang, T. Zhou, Y. Jing, Effects of $BaCu(B_2O_5)$ on sintering characteristics and microwave dielectric properties of $CaWO_4$ ceramics. Ceram. Int. **40**(7), 10531–10535 (2014)
5. H. H. Xi, D. Zhou, H. D. Xie, B. He, Q. P. Wang, Raman spectra, infrared spectra, and microwave dielectric properties of low-temperature firing $[(Li_{0.5}Ln_{0.5})_{1-x}Ca_x]MoO_4$(Ln = Sm and Nd) solid solution ceramics with scheelite structure, J. Am. Ceram. Soc. **98** (2), 587–593 (2015)
6. L.X. Pang, D. Zhou, W.G. Liu, Low-temperature sintering and microwave dielectric properties of $CaMoO_4$-based temperature stable LTCC material. J. Am. Ceram. Soc. **97**(7), 2032–2034 (2014)
7. D. Zhou, H. Wang, Q. P. Wang, X. G. Wu, Ju Guo, G. Q. Zhang, L. Shui, X. Yao, Microwave dielectric properties and Raman spectroscopy of scheelite solid solution $[(Li_{0.5}Bi_{0.5})_{1-x}Ca_x]MoO_4$ ceramics with ultra-low sintering temperatures, Funct. Mater. Lett. **03** (04), 253–257 (2010)
8. H. Zhou, H. Wang, K. Li, M. Zhang, H. Yang, Microwave dielectric properties of low temperature firing $(Li_{1/2}Nd_{1/2})WO_4$ ceramic. J. Mater. Sci. Mater. Electron. **21**(3), 252–255 (2009)
9. T. Hong, Y.D. Hu, S.X. Bao, C. Luo, L. Ai, P.B. Jiang, J. Chen, Z.Z. Duan, Low-temperature sintering and microwave dielectric properties of $CaMoO_4$ ceramics. J. Electron. Mater. **48**(2), 972–976 (2018)
10. E.S. Kim, S.H. Kim, B.I. Lee, Low-temperature sintering and microwave dielectric properties of $CaWO_4$ ceramics for LTCC applications. J. Eur. Ceram. Soc. **26**(10–11), 2101–2104 (2006)
11. D. Zhou, J. Guo, X. Yao, Phase evolution and microwave dielectric properties of $(Li_{0.5}Bi_{0.5})(W_{1-x}Mo_x)O_4$ $(0.0 \le x \le 1.0)$ ceramics with ultra-low sintering temperatures, Funct. Mater. Lett. **05** (04), 1250042 (2012)
12. Z. Zhang, H. Sun, X. Tang, H. Zhang, T. Zhou, Y. Jing, Glass-free low-temperature sintering and microwave dielectric properties of $CaWO_4$–Li_2WO_4 ceramics. Ceram. Int. **40**(1), 1613–1617 (2014)
13. F. Gu, G. Chen, X. Kang, X. Li, C. Zhou, C. Yuan, Y. Yang, T. Yang, A new $BiVO_4$/$Li_{0.5}Sm_{0.5}WO_4$ ultra-low firing high-k microwave dielectric ceramic, J. Mater. Sci. **50** (3), 1295–1299 (2014)
14. M. Guo, Y. Li, G. Dou, J. Lin, A new microwave dielectric ceramics for LTCC applications: $Li_2Mg_2(WO_4)_3$ ceramics. J. Mater. Sci. Mater. Electron. **25**(9), 3712–3715 (2014)
15. L. X. Pang, D. Zhou, J. Guo, Z. X. Yue, X. Yao, Microwave dielectric properties of $(Li_{0.5}Ln_{0.5})MoO_4$ (Ln = Nd, Er, Gd, Y, Yb, Sm, and Ce) ceramics, J. Am. Ceram. Soc. **98** (1), 130–135 (2015)
16. G. H. Chen, F. F. Gu, M. Pan, L. Q. Yao, M. Li, X. Chen, Y. Yang, T. Yang, C. L. Yuan, C. R. Zhou, Microwave dielectric properties of $BiVO_4$/$Li_{0.5}Re_{0.5}WO_4$ (Re = La, Nd) ultra-low firing ceramics, J. Mater. Sci. Mater. Electron. **26** (9), 6511–6517 (2015)
17. H. Guo, L. Fang, X. Jiang, J. Li, F. Lu, C. Li, A novel low-firing and low loss microwave dielectric ceramic $Li_2Mg_2W_2O_9$ with corundum structure. J. Am. Ceram. Soc. **98**(12), 3863–3868 (2015)
18. L. X. Pang, D. Zhou, Z. X. Yue, Temperature independent low firing $[Ca_{0.25}(Nd_{1-x}Bi_x)_{0.5}]MoO_4$ $(0.2 \le x \le 0.8)$ microwave dielectric ceramics, J. Alloy. Comp. **781**, 385–388 (2019)
19. M.M. Krzmanc, M. Logar, B. Budic, D. Suvorov, Dielectric and microstructural study of the $SrWO_4$, $BaWO_4$, and $CaWO_4$ scheelite ceramics. J. Am. Ceram. Soc. **94**(8), 2464–2472 (2011)
20. L. Cheng, P. Liu, S.X. Qu, H.W. Zhang, Microwave dielectric properties of AWO_4 (A=Ca, Ba, Sr) ceramics synthesized via high energy ball milling method. J. Alloy. Comp. **581**, 553–557 (2013)
21. J. J. Bian, J. Y. Wu, Designing of glass-free ltcc microwave ceramic- $Ca_{1-x}(Li_{0.5}Nd_{0.5})_xWO_4$ by crystal chemistry, J. Am. Ceram. Soc. **95** (1), 318–323 (2012)
22. H. Yang, Y. Lin, J. Zhu, F. Wang, Z. Dai, A new $Li_{0.5}Sm_{0.5}WO_4$ low temperature firing microwave dielectric ceramic, J. Alloy. Comp. **502** (2), L20-L23 (2010)
23. E.S. Kim, B.S. Chun, R. Freer, R.J. Cernik, Effects of packing fraction and bond valence on microwave dielectric properties of $A^{2+}B^{6+}O_4$ (A^{2+}: Ca, Pb, Ba; B^{6+}: Mo, W) ceramics. J. Eur. Ceram. Soc. **30**(7), 1731–1736 (2010)
24. R.D. Shannon, Revised effective ionic radii and systematic studies of interatomic distances in halides and chalcogenides. Acta Crystallogr. A **32**, 751–767 (1976)
25. Z. Fang, B. Tang, Y. Yuan, X. Zhang, S. Zhang, Structure and microwave dielectric properties of the $Li_{2/3(1-x)}Sn_{1/3(1-x)}Mg_xO$ systems (x = 0-4/7). J. Am. Ceram. Soc. **101**(1), 252–264 (2018)
26. Z. Fang, B. Tang, F. Si, E. Li, H. Yang, S. Zhang, Phase evolution, structure and microwave dielectric properties of $Li_{2+x}Mg_3SnO_6$ (x = 0.00–0.12) ceramics, Ceram. Int. **43** (16),13645–13652 (2017)
27. H. Xiang, L. Fang, W. Fang, Y. Tang, C. Li, A novel low-firing microwave dielectric ceramic $Li_2ZnGe_3O_8$ with cubic spinel structure. J. Eur. Ceram. Soc. **37**(2), 625–629 (2017)
28. Q. Liao, L. Li, X. Ren, X. Ding, New low-loss microwave dielectric material $ZnTiNbTaO_8$. J. Am. Ceram. Soc. **94**(10), 3237–3240 (2011)
29. N. X. Xu, J. H. Zhou, H. Yang, Q.L. Zhang, M.J. Wang, L. Hu, Structural evolution and microwave dielectric properties of MgO-LiF co-doped Li_2TiO_3 ceramics for LTCC applications, Ceram. Int. **40** (9), 15191–15198 (2014)
30. G. Zhang, J. Guo, H. Wang, Ultra-low temperature sintering microwave dielectric ceramics based on Ag_2O-MoO_3 binary system. J. Am. Ceram. Soc. **100**(6), 2604–2611 (2017)
31. M. Guo, Y. Li, G. Dou, S. Gong, Low-temperature sintered $ZnNb_2O_6$–$CaTiO_3$ ceramics with near-zero τ_f. Mater. Chem. Phys. **147**(3), 728–734 (2014)